An Integrated Systems Model for Heavy Ion Drivers

W. R. Meier
R. O. Bangerter
A. Faltens

September 2, 1998

DISCLAIMER

Paper: SO07

An Integrated Systems Model for Heavy Ion Drivers*

W.R. Meier
Lawrence Livermore National Laboratory, Livermore, CA 94551, USA

R.O. Bangerter and A. Faltens
E.O. Lawrence Berkeley National Laboratory, Berkeley, CA 94720, USA

Abstract

A source-to-target computer model for an induction linac driver for heavy ion fusion has been developed and used to define a reference case driver that meets the requirements of one current target design. Key features of the model are discussed, and the design parameters of the reference case design are described. Examples of the systems analyses leading to the point design are given, and directions for future work are noted.

Key Words: heavy ion, inertial confinement, fusion, driver, accelerator, systems model

PACS: 28.52.-s Fusion reactors
29.17.+w Electrostatic, collective, and linear accelerators

Send proofs to:

Wayne R. Meier
Lawrence Livermore National Laboratory
P.O. Box 808, L-481
Livermore, CA 94551
USA

Fax: 510-422-7390
Phone: 510-422-8536
E-mail: wmeier@llnl.gov

1. Introduction

The heavy ion fusion programs at Lawrence Livermore National Laboratory and E.O. Lawrence Berkeley National Laboratory have been collaborating on the development of a computer model for systems analysis of heavy ion drivers based on induction linac technology. Work to date has focused on drivers for future heavy ion fusion (HIF) power plants, but the tools being developed will also be used to evaluate candidates for more near-term experimental facilities. Previous systems modeling and conceptual design studies for HIF drivers can be found in [1-4]. The model described here is an integrated source-to-target model that includes the key interdependencies of the major subsystems in terms of cost, performance and constraints. In this paper, we give a brief description of the general features of the model, including some example parametric studies, present the reference case design parameters, and conclude with the results of some cost sensitivity studies and directions for future work.

2. Model description and example parameter studies

2.1. General features

The computer model is written using a commercial scientific/engineering software package called Mathcad [5] that incorporates text and graphics in an easily readable and user-friendly format. The reference case induction linac driver architecture includes a multi-beam injector feeding an electrostatic-focusing accelerator section, four-to-one beam merging and transition to a magnetic-focusing accelerator section at some higher energy (e.g., ~100 MeV). The main accelerator is followed by final transport and final focus sections. The final transport section

provides the distance needed for drift compression (to get the required pulse length on target) and re-alignment of the beams for two-sided illumination. The final focus section includes the final focus quadrupoles that are used to first expand the beam radially and then focus it to a small spot on target. Calculation of the spot size on target is included.

The heart of the model is the set of transport, component sizing, and cost scaling algorithms that describe the components in each section of the driver. Numerous inputs, assumptions and constraints for the models of the various components are defined throughout the program. Typical assumptions are cost scaling dependencies and component unit costs (e.g., $/kg of various materials). Examples of constraints include the source current density limit (A/m^2) and the acceleration gradient limit (V/m) in the accelerator. A key input is the specification of beam characteristics that the driver must deliver to the target. Table 1 gives the target requirements for one current HIF target design [6]; other target designs will be investigated in future work. Note that the target requires a prepulse with a lower ion energy (3 GeV) than the main pulse (4 GeV).

2.2. Injector

The multi-beam injector delivers ions at 2 MeV simultaneously to each beam channel in the low-energy, electrostatic-focusing section of the accelerator. Eventually, the injector voltage will be determined by comparing the cost of the injector as a function of voltage to the cost of induction acceleration at low voltage and picking the lowest cost approach. For now, we are assuming a 2 MeV injector because that is our present experience. The total charge that must be transported is calculated from the energy on target and final voltages of the prepulse and main pulse beams. The initial current per beam at the exit of the injector is the charge per beam

3

divided by the initial pulse duration, which is one of the design variables we optimize. In our model, the number of prepulse and main pulse beams is set so that each beam carries the same charge. In this way, the entire accelerator up to 3 GeV is identical for prepulse and main pulse beams. The source radius for each beam depends on the achievable source current density (A/m^2), which is a function of diode gap as described by the Child-Langmuir law and is constrained by emission limits for the particular ion source. Since for good optics the diode gap is proportional to the source radius, there is a unique combination of source radius, diode gap, and diode voltage that gives the required current per beam. For example, the reference case design with 192 beams at the low energy end has a source radius of 29 mm, diode gap of 73 mm, and a diode voltage of ~300 kV, providing a current of 0.3 A per beam at a 30 μs pulse duration.

2.3. Electrostatic focusing section

Electrostatic quadrupoles are used at the low energy end of the accelerator, from the 2 MeV injector energy to ~100 MeV in our reference case design. The general configuration of a multi-beam array is illustrated in Fig. 1. (For simplicity and clarity, Fig. 1 shows a 32-beam array instead of the 192-beam array used as our reference design. The 192 beams will be configured in a similar pattern.) The beam size depends on the current per beam coming from the injector. Electrode dimensions are scaled from the beam size and in turn determine the outer radius of the multi-beam array and the inner radius of the induction cores. Here we find the inner radius decreases with increasing number of beams and increasing initial pulse duration. For our reference case of 192 beams and 30 μs, the inner radius of the cores is 0.37 m.

The acceleration gradient increases from an initial value of ~50 kV/m to 330 kV/m at 100 MeV; it is limited by the maximum allowable radial build of the cores, which is a user specified constraint (1.0 m in this case). This then determines the length of the accelerator required to achieve a given ion energy, which is 492 m to an ion energy of 100 MeV.

The cost of the electrostatic quadrupoles is broken down into six subsystems: electrodes, end plates, insulators, power supplies, vacuum vessel, and articulation. The cost of the accelerator modules (or cores) includes the cost of magnetic material, cell housing, structural support, and gap insulators. The electrostatic focusing section cost is the sum of the costs for quadrupoles, cores, pulsed power and the vacuum pumping systems. To this we add the cost of the injector to get the cost of the front end. Cost scaling relationships have been developed for all these subsystems.

Fig. 2 shows the cost of the front end as a function of the initial pulse duration. The costs have been normalized to the minimum, which occurs at 30 μs. The cost is strongly dominated by the cost of cores for pulse durations greater than 30 μs. At lower pulse durations, the injector cost rises rapidly due to the higher initial current per beam and correspondingly high source area requirements. The cost of the front end also decreases with increasing number of beams, but reaches diminishing returns beyond 150-200 beams. The front end cost of our 192-beam reference case design is only 10% higher than a 300 beam case.

2.4. Magnetic focusing section

At the transition from electrostatic to magnetic focusing, the multi-beam array undergoes a four-to-one beam merging, which gives 48 beams in the magnetic section. The transition energy is a design variable that is chosen to minimize the overall driver cost (including front end, magnetic focusing section, final transport and final focusing). As will be shown later, the cost is rather insensitive to this transition energy over 10's of MeV, with the optimum at ~ 100 MeV.

As in the electrostatic section, all of the beams in the magnetic quadrupole section share common cores. Each quadrupole occupies a square unit cell, illustrated in Fig. 3, consisting of an inner vacuum pipe (bore) wall, a 0.5-cm-thick layer of superinsulation, a support pipe wall on which the superconductor is wound, and regions (primarily the corners of the square) for superconductor and associated cooling. The entire package is surrounded by a structural metal box on the outer edge. The inner radius of the bore is scaled from the beam size, which depends on the current per beam and the magnetic field of the quadrupole. The thicknesses of the pipe walls and the outer box wall scale in proportion to the beam size and are set by stress considerations. One half of a unit cell thickness of conductor surrounds the entire array to provide a flux return path for the quadrupoles on the outer edge.

The overall radial dimension of the array determines the inner radius of the induction cores. Fig. 4 shows the core radius as a function of the quadrupole field at the winding, B_W, for several different initial pulse durations. The minimum inner radius occurs at 6 T in each case. At higher fields, extra space is needed for the conductor, and the quadrupole unit cell and overall array dimensions increase. While 6 T gives the smallest core radius, the minimum cost for the driver occurs at $B_W = 4$ T. This illustrates the importance of an integrated model.

As shown in Fig. 5, the acceleration gradient in the magnetic focusing section increases rapidly to 1 MV/m and then rises slowly to a maximum of nearly 2 MV/m. As the acceleration gradient is increased, the core axial packing fraction is decreased to reduce capacitance and prevent breakdown. Once the ions reach 3 GeV, the array is split into two parallel multi-beam arrays, one for the prepulse (16 beams) and one for the main pulse (32 beams). As the main pulse beams continue to accelerate to 4 GeV, the prepulse beams are simply transported to the end of the accelerator.

2.5. Final transport and focusing

At the end of the accelerator, the prepulse and main pulse have pulse durations of 140 and 110 ns, respectively. These must be shortened to 30 and 8 ns, respectively, prior to focusing on target. A simple model is used to calculate the required velocity tilt and drift length to accomplish this [7]. Secondly, we determine the transport length needed simply to redirect the beams to a two-sided illumination geometry as a function of the field in the dipole bending magnets. The larger of the two distances sets the final transport length. The final transport cost includes the costs of quadrupoles, dipoles, and a vacuum system. In our reference case, a dipole field of 4.5 T gave the minimum cost and resulted in final transport length (from the end of the accelerator to the end of the final focus magnets) of 415 m. Note that as the pulses are compressed, the current per beam rises rapidly, and the bore radius and quadrupole fields are increased in order to transport the higher currents.

The final focus geometry is based on a simple point-to-point lens model consisting of four quadrupoles for each beam [8]. Magnet dimensions and costs scale with the beam size at the middle of the final quadrupole, which is equal to the product of the beam focusing half angle, θ_f, and the final focus length, L_f (distance from the middle of the last quadrupole to the target). An allowance for neutron shielding inside the bore of the final focus quadrupoles is included, although more detailed work is needed on this aspect of the design. The inner radius of the bore is also constrained by voltage breakdown between the beam and bore wall, using a limit of 200 kV/cm, which is adequate for short duration pulses.

3. Reference case parameters

Table 2 shows several parameters of the reference case design which delivers the required 5.9 MJ to the target. The overall length of the accelerator is 3250 m plus an additional 415 m for the final transport and focusing. The current per beam increases from 0.3 A at the exit of the injector to 1.1 kA for the prepulse and 4.2 kA for the main pulse. The beam radius is less than 7 mm in both the electrostatic and magnetic focusing sections, and the bore radius is ~ 13 mm.

4. Cost results

4.1. Cost breakdown

The total direct cost of the 5.9 MJ reference case driver is ~ $1.4 B. As indicated in Fig. 6, the contributions to this total are: injector (2%), electrostatic focusing section (10%), magnetic

focusing section (48%), final transport (6%), and final focus (3%). We include an allowance for instrumentation and control (6%) and installation and assembly (23%). We note that these results are preliminary, and work continues on refining the cost scaling models and accelerator architecture in order to reduce this cost. If we examine the cost of the magnetic focusing section in more detail, we find that its cost is dominated by the cost of cores (40%) and pulsed power (40%). The quadrupoles and vacuum system account for 14% and 6%, respectively.

4.2. Cost sensitivity

We have also examined the sensitivity of the driver cost to changes in reference point design variables and have found that the cost is relatively insensitive to parameter variations over a rather broad range. The driver cost is most sensitive to reducing the initial pulse duration (+17% going to 15 μs) and reducing the number of beams (+13% for half as many beams). Changing the quadrupole field over the range of 2 to 6 T increases the cost by 5% or less. The transition energy from electrostatic to magnet focusing has very little impact over the range of 50 to 150 MeV.

5. Future work

This work is still in progress, and several things are planned for the future. First, we will conduct studies with the current architecture to find optimum designs and costs for different ions, ion energies and targets, including higher charge-to-mass ratio ions. We will work to improve the cost basis and cost scaling models, develop a better treatment of emittance growth along the accelerator, and provide more detail on the final focusing model. Technical solutions, such as

using fewer, more powerful thyratrons for the pulsed power at the high energy end, will also be incorporated. Finally, we plan to evaluate other architectures (e.g., an all-magnetic front end, elimination of merging, replacing part of the magnetic section with a recirculating linac).

Acknowledgments

References

[1] D.J. Dudziak, W.W. Saylor, and W.B. Herrmannsfeldt, "U.S. heavy-ion fusion systems assessment project overview," *Fusion Technol.*, **13**, (Feb. 1988) 207.

[2] D.S. Zuckerman, D.E. Driemeyer, L.M. Waganer, and D.J. Dudziak, "An induction linac driven heavy-ion-fusion systems model," *Fusion Technol.*, **13** (Feb. 1988) 217.

[3] J. Hovingh, V.O. Brady, A. Faltens, and D. Keefe, and E.P. Lee, "Heavy-ion linear induction accelerators as drivers for inertial fusion power plants," *Fusion Technol.*, **13** (Feb. 1988) 255.

[4] R.L. Bieri, M.J. Monsler, W.R. Meier, and L.Stewart, "Heavy-ion driver design and scaling," *Fusion Technol.*, **21** (May 1992) 1583.

[5] Mathcad is a registered trademark of MathSoft, Inc., 101 Main St. Cambridge, MA 02142, USA, Phone: 800-628-4223, Ineternet: www.mathsoft.com.

[6] M. Tabak and D. Callahan-Miller, "Distributed radiator heavy ion target designs," these Proceedings.

[7] E.P. Lee, C. Fong, S. Mukherjee, and W. Thur, "Conceptual design of bend, compression and final focus components of ILSE," IEEE report CH2669-0/89/0000-0971 (1989).

[8] E.P. Lee, "Heavy ion driven LMF design concept," LBNL report LBL-31248 revised (July 1995).

<div align="center">

Table 1
Target requirements

</div>

	Prepulse	Main Pulse
Ion mass, amu	200	200
Ion energy, GeV	3.0	4.0
Beam energy, MJ	1.6	4.3
Total charge, mC	0.53	1.07
Pulse duration on target, ns	30	8
Spot radius on target, mm	2.7	2.7

<div align="center">

Table 2
Reference case design parameters

</div>

Number of beams (electrostatic / magnetic)	192 / 48
Initial pulse duration, μs	30
Transition to magnetic focusing, MeV	100
Accelerator quadrupole field at winding, T	4.0
Final transport quad field at winding, T	4.5
Final focus length, m	5.0
Beam focus half angle, mrad	10

Along accelerator

	Injector Exit	End of EQF[a]	Pre-pulse	Main Pulse
Ion energy, GeV	0.002	0.1	3.0	4.0
Pulse duration, μs	30	4.2	0.14	0.11
Pulse length, m	41.7	41.7	7.6	6.6
Beam current, A	0.3	2.0	230	310
Beam radius, mm	6.6	6.6	6.9	6.9
Bore radius, mm	12.6	12.6	12.9	12.9
Core inner radius, m	0.37	0.37	0.29	0.25
Core build, m	0.92	1.0	0.89	0.4
Accel. gradient, MV/m	0.05	0.33	1.77	1.91
Dist. from injector, m	0	490	2220	3250

At last final focus quadrupole

	Prepulse	Main Pulse
Pulse duration, ms	30	8
Pulse length, m	1.6	0.5
Beam current, A	1110	4170
Beam radius, mm	50	50
Bore radius, mm	70	70

[a]EQF = Electrostatic quadrupole focusing

Core

Electrode / beam geometry

Electrode

Beam

P

R_e

a_b R_b

a_b = average beam radius
R_b = 1.91 a_b = bore radius
R_e = 1.14 R_b = electrode radius
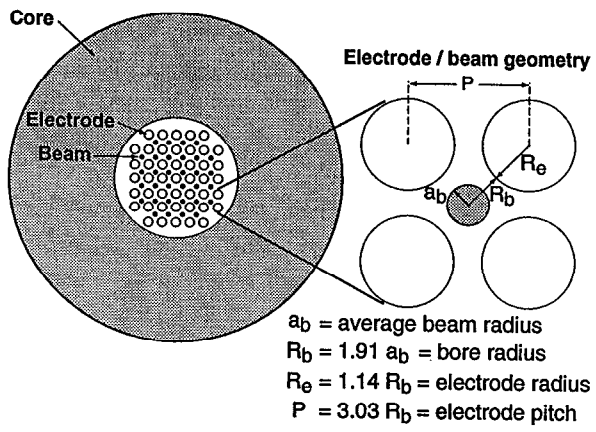P = 3.03 R_b = electrode pitch
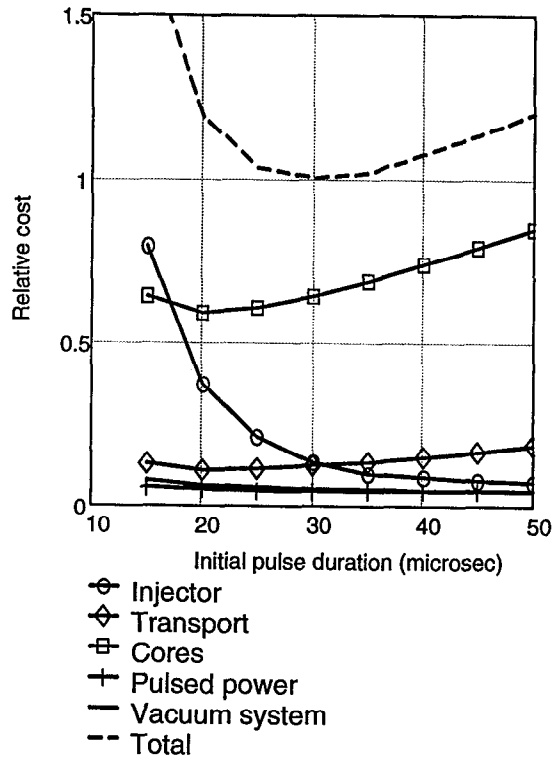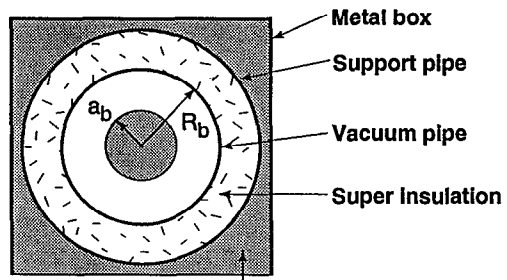
Fig. 1. Configuration of electrostatic quadrupole array.

13

Fig. 2. Relative cost of front end (up to 100 MeV) as a function of initial pulse duration for 192 beam case.
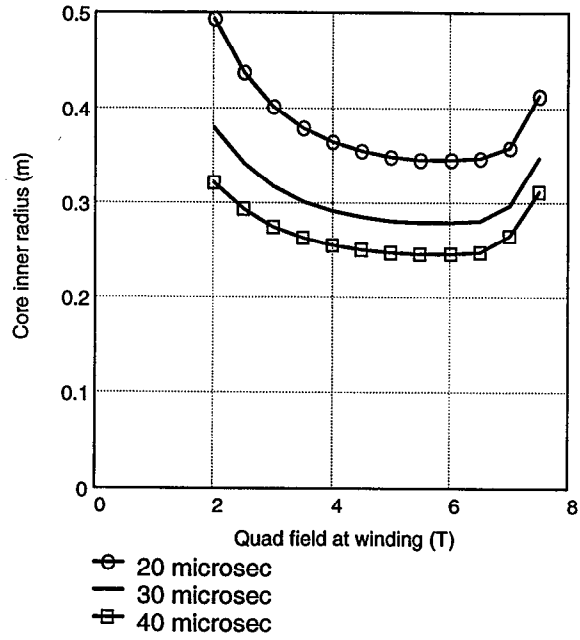
Fig. 3. Configuration of magnetic quadrupoles.

Fig. 4. Core inner radius as a function of the quadrupole field at the winding for initial pulse durations of 20, 30 and 40 μs.
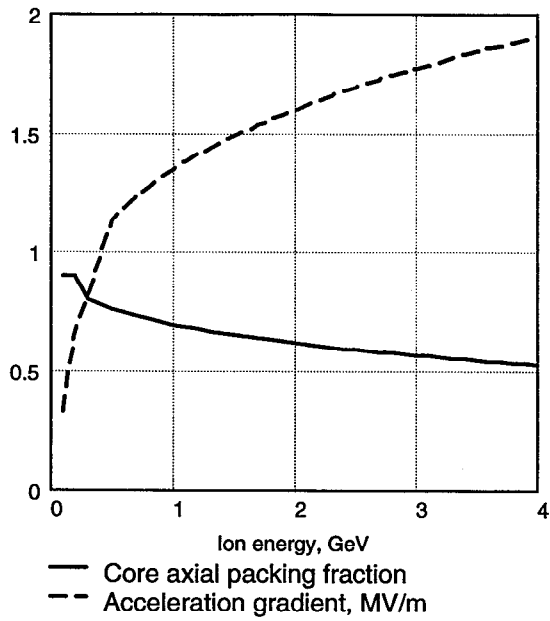
Fig. 5. Acceleration gradient and core axial packing fraction as a function of ion energy in the magnetic focusing section.
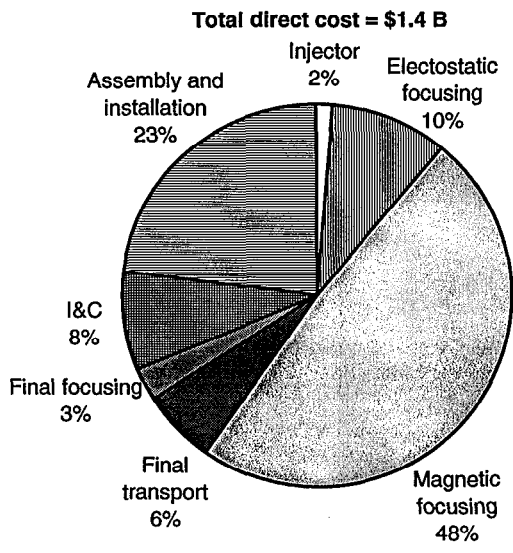
Fig. 6. Cost breakdown for reference case design.

List of figure captions

Fig. 1. Configuration of electrostatic quadrupole array.

Fig. 2. Relative cost of front end (up to 100 MeV) as a function of initial pulse duration for 192 beam case.

Fig. 3. Configuration of magnetic quadrupoles.

Fig. 4. Core inner radius as a function of the quadrupole field at the winding for initial pulse durations of 20, 30 and 40 μs.

Fig. 5. Acceleration gradient and core axial packing fraction as a function of ion energy in the magnetic focusing section.

Fig. 6. Cost breakdown for reference case design.